

Cycle 10 Phase II Update for STIS

In this Update...

Mama Imaging Snapshots in Cycle 10 / 1
Update on the STIS CCD CTE Performance / 2
New Pseudo-Apertures for Improved CTE on Spectroscopy of Faint Targets / 4
Update on the Sensitivity Monitoring / 6
Echelle Scattered Light Correction / 8

STIS has been operating without major changes in its performance since the release of the STIS Instrument Handbook (IHB) version 4.1. This update provides the latest information regarding STIS performance and policies which are relevant to the preparation of Cycle 10 Phase II proposals. The items presented here may also be found on the STIS web page at <http://www.stsci.edu/instruments/stis>. As always, new information will be regularly described in the Spectrographs STAN (Space Telescope Analysis Newsletter) and posted on the web pages. General help or documentation may be obtained by sending email to help@stsci.edu.

This update should be used in conjunction with the STIS IHB v4.1 and the Cycle 10 Phase II Proposal Instructions to aid you in the completion of your Phase II proposal for Cycle 10. If you have specific questions not covered in the documents, you should consult your Program Coordinator, Contact Scientist (if one has been assigned), or send email to help@stsci.edu.

Mama Imaging Snapshots in Cycle 10

When the STIS IHB v4.1 was released, the Advanced Camera for Surveys (ACS) was planned to be operational in Cycle 10. ACS's imaging capabilities are in many cases complementary, in some cases even superior,

to those of STIS. In particular it was expected that ACS would be the instrument of choice for Snapshot programs in the ultraviolet, mainly because of the larger field of view of the ACS. The strict bright object protection policies for STIS require a significant amount of implementation resources for STIS MAMA imaging observations. Since only a very small fraction of planned STIS Snapshot images is actually executed, it was felt that the amount of implementation resources is not justified by the small execution probability and due to the availability of ACS.

ACS will not be available for observations in Cycle 10. At the same time, STScI has developed applications to automatize the bright object checking of MAMA imaging fields using the Guide Star Catalog II. Therefore MAMA imaging Snapshots will be allowed during Cycle 10 --- contrary to what is stated in the IHB v4.1. Note, however, that we do not expect the execution probabilities of MAMA imaging Snapshots to be higher than in previous cycles. General Observers will have the main responsibility for providing all the required bright object information in preparation of their Cycle 10 Phase II proposals.

Update on the STIS CCD CTE Performance

Our annual determination of the Charge Transfer Efficiency (CTE) of the STIS CCD has indicated a significant deterioration of the parallel-register Charge Transfer Inefficiency ($CTI = 1 - CTE$). The results reported here represent measurements performed on Oct. 13, 2000, i.e., after 3.6 years on-orbit.

It should be noted at the outset that CTE effects have not been incorporated into the STIS Exposure Time Calculators (ETCs) as yet. Thus, should you believe the CTE losses described herein may impact your program, you will need to provide longer exposure times in your Cycle 10 Phase II proposal to compensate for the anticipated losses. In particular, Cycle 10 observers using the STIS CCD to observe faint targets (especially spectroscopy of point sources or imaging of faint point sources) with less than a few hundred counts (integrated over an aperture of 5 pixels diameter) above a low background are advised to adjust their exposure times appropriately, within the restrictions of their allocated orbits. Furthermore, observers using the CCD for spectroscopy of sources having a spatial extent less than about 3 arcsec are urged to use the pseudo-apertures located near row 900 of the CCD.

Table 1: CTI Values for the STIS CCD after 2.5 and 3.6 years in orbit.

Intensity (e ⁻)	Sky (e ⁻ /pix)	CTI (15 Sep 99)	CTI (13 Oct 00)
150 ± 50	3	(2.33 ± 0.38) × 10 ⁻⁴	(2.73 ± 0.27) × 10 ⁻⁴
	6	(1.72 ± 0.40) × 10 ⁻⁴	(1.90 ± 0.37) × 10 ⁻⁴
350 ± 100	3	(1.77 ± 0.19) × 10 ⁻⁴	(1.99 ± 0.18) × 10 ⁻⁴
	6	(1.39 ± 0.18) × 10 ⁻⁴	(1.42 ± 0.19) × 10 ⁻⁴
	15	(0.54 ± 0.26) × 10 ⁻⁴	(1.35 ± 0.34) × 10 ⁻⁴
1000 ± 50	3	(1.39 ± 0.11) × 10 ⁻⁴	(1.49 ± 0.10) × 10 ⁻⁴
	6	(1.15 ± 0.09) × 10 ⁻⁴	(1.13 ± 0.08) × 10 ⁻⁴
	15	(0.57 ± 0.08) × 10 ⁻⁴	(0.92 ± 0.10) × 10 ⁻⁴
	30	(0.57 ± 0.09) × 10 ⁻⁴	(0.61 ± 0.08) × 10 ⁻⁴
5000 ± 1000	3	(5.77 ± 0.57) × 10 ⁻⁵	(7.88 ± 0.36) × 10 ⁻⁵
	6	(5.39 ± 0.35) × 10 ⁻⁵	(7.78 ± 0.30) × 10 ⁻⁵
	15	(3.94 ± 0.38) × 10 ⁻⁵	(5.34 ± 0.40) × 10 ⁻⁵
	30	(3.79 ± 0.47) × 10 ⁻⁵	(5.10 ± 0.42) × 10 ⁻⁵
10000 ± 2000	3	(4.14 ± 0.41) × 10 ⁻⁵	(5.23 ± 0.18) × 10 ⁻⁵
	6	(3.70 ± 0.55) × 10 ⁻⁵	(4.76 ± 0.18) × 10 ⁻⁵
	15	(3.36 ± 0.28) × 10 ⁻⁵	(3.88 ± 0.29) × 10 ⁻⁵
	30	(3.03 ± 0.29) × 10 ⁻⁵	(3.34 ± 0.25) × 10 ⁻⁵
30000 ± 7000	3	(2.63 ± 0.59) × 10 ⁻⁵	(3.43 ± 0.18) × 10 ⁻⁵
	6	(3.04 ± 0.29) × 10 ⁻⁵	(3.36 ± 0.18) × 10 ⁻⁵
	15	(2.50 ± 0.21) × 10 ⁻⁵	(2.91 ± 0.14) × 10 ⁻⁵
	30	(2.49 ± 0.20) × 10 ⁻⁵	(2.50 ± 0.11) × 10 ⁻⁵

The CTE test described here employed imaging observations of a sparse star field and was executed with the STIS CCD in Clear mode (50CCD) and using CCDGAIN = 1. The observations were taken in the CVZ and using two exposure times (20 s and 100 s) in order to study the dependence of CTE to the sky background. All images were alternatively read out by two amplifiers, located on opposite sides of the CCD. The subsequent analysis consisted of aperture photometry of all sufficiently uncrowded stars in the field with intensities higher than 4σ above the background. A circular aperture with a radius of 2 pixels was used, centered on the stars. The CTI follows from the slope of the relation between the ratio of the count rates of stars in images read out by the two amplifiers and the Y coordinate (i.e., the CCD row number). The results of the analysis are provided in Table 1 where the CTI values (in units of relative charge lost per pixel) are listed as a function of the sky background and the object intensity within the aperture. The CTI results are listed for two epochs: 2.5 and 3.6 years after launch.

Comparing the results of the two epochs, it can be seen that the CTI is increasing by $\sim 15\%$ per year on average. This can be used as a rule of thumb for estimating exposure times in Cycle 10.

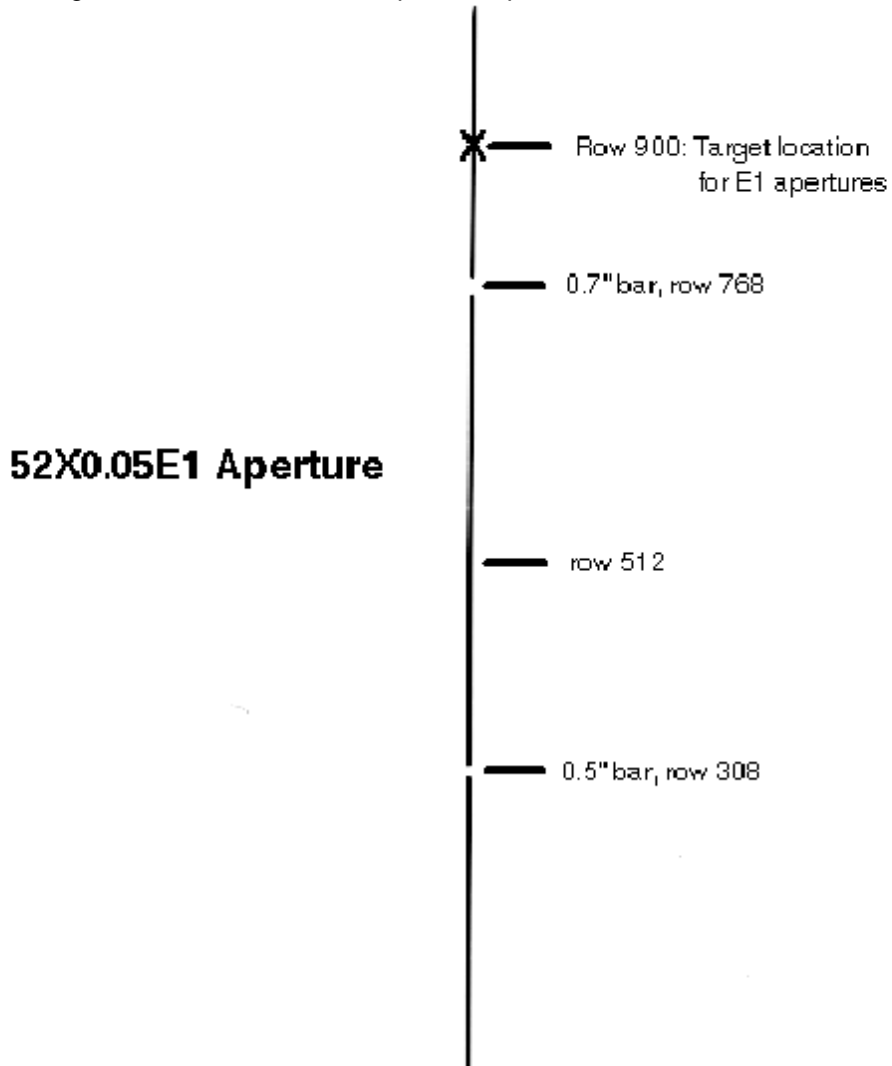
Further analyses of CTE effects on imaging and spectroscopic observations of extended objects (e.g., galaxies) will be performed during the remainder of Cycle 9, and will be reported as STIS Instrument Science Reports on the web.

New Pseudo-Apertures for Improved CTE on Spectroscopy of Faint Targets

Decreasing charge transfer efficiency in the STIS CCD has a detrimental effect on faint spectra acquired at the default location at the center of the chip. For sources with fluxes less than $\sim 1 \times 10^{-16} \text{ erg cm}^{-2} \text{ s}^{-1} \text{ \AA}^{-1}$, less than ~ 100 electrons are accumulated per pixel in exposure times of 1000 s or less. (This is the longest integration time we recommend due to the deleterious impact of multiple cosmic rays in a CR-SPLIT at longer integration times.) At signal levels of 50-100 e^- , 15% or more of the charge can be lost during readout due to charge-transfer inefficiencies (see page 7-121 of the STIS Instrument Handbook, and updated information on CTE in this handout). Many STIS science programs have fluxes in this range.

For spectra of point sources and compact objects such as galactic nuclei, the full length of the slit is not needed. A target location closer to the read-out amplifier near the end of the slit can decrease the charge lost during parallel transfers by a factor of ~ 5 . One could achieve this offset through the use of offset targets or appropriate POS TARG entries on the Phase II proposal, but these methods are a bit cumbersome and can be prone to error. We have therefore defined a set of “pseudo-apertures” that use the same physical long slits available for STIS CCD observations, but have their default target placement near row 900, ~ 5 arcseconds from the top of the STIS CCD. This is schematically illustrated in Figure 1. Observers can use these new aperture names to place their targets at this location in a rather transparent fashion.

Figure 1: Location of the new pseudo apertures.



The new aperture names and the approximate Y location of the resulting spectra are given in Table 2. Using these aperture names, observers can perform an ACQ/PEAK, target offset, and a POS TARG just as they would for the standard aperture names that locate targets near the center of the slit. The new apertures are also recognized by the calibration pipeline software, so spectra are extracted from the correct location using appropriate wavelength solutions, spectral traces, and background regions. For optimum throughput when using these apertures, we recommend using an ACQ/PEAK exposure to center the target in the aperture when using aperture 52X0.1E1 and 52X0.05E1.

Table 2: New aperture names and the approximate Y location of the resulting spectra.

Aperture	Y Location	ACQ/PEAK?
52X2E1	894	no
52X0.5E1	893	no
52X0.2E1	893	no
52X0.1E1	898	yes
52X0.05E1	898	yes

While use of these apertures will ameliorate CTE losses, we caution observers to carefully assess the potential impact on their science programs due to the decreased spatial coverage and the relative locations of the bars on the slit.

Update on the Sensitivity Monitoring

The analysis of the STIS Sensitivity Monitor observations from 1997 through October 1, 2000 shows continuing sensitivity trends correlated with time for all first-order low and medium resolution modes as well as a temperature dependence in the FUV. The mean wavelength-averaged rate of sensitivity loss for the L-modes is $\sim 1\%/yr.$, with individual losses ranging from $\sim 0\%/yr.$ (G430L, G750L) to $\sim 1.5\%/yr.$ (G140L, G230L, G230LB). Selected wavelength settings of the M-modes have an average sensitivity loss of almost $2\%/yr.$, with individual losses ranging from $\sim 1\%/yr.$ (G230M, G430M, G750M) to $\sim 3.5\%/yr.$ (G230MB). Elimination of cosmic rays may be compromised, especially if using only a few sub-pixel offsets with just one image at each location.

Figures 2 through 4 present the relative sensitivity vs. time for each observing mode, plus the linear fits to those points. The slope, i.e., percent change in sensitivity per year, and its 1σ uncertainty in the fits are given at the bottom of each figure. The $1-\sigma$ rms (%) of the data residuals from the linear fit is given by the SIGMA value also at the bottom of each figure.

Figure 2: Sensitivity decrease measured with the G140L grating.

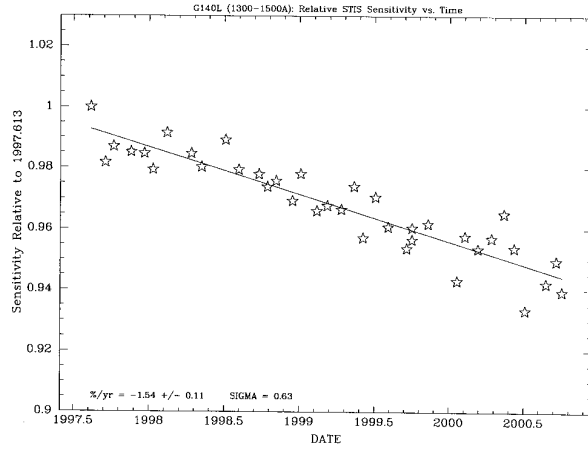


Figure 3: Sensitivity decrease measured with the G230L grating.

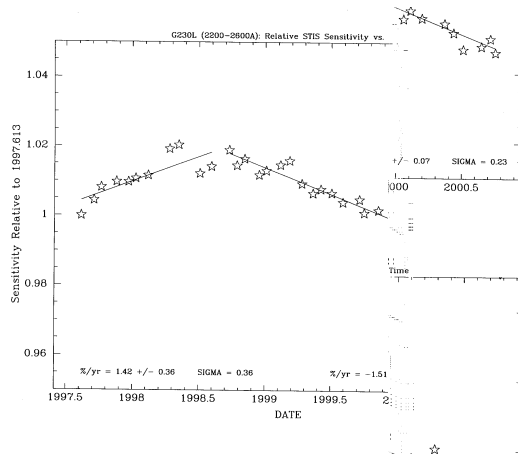
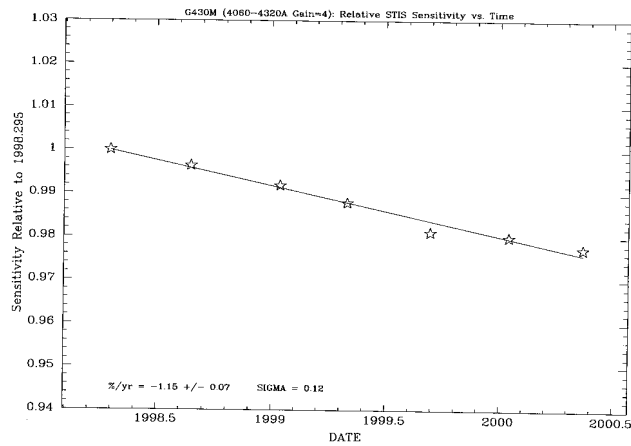


Figure 4: Sensitivity decrease measured with the G430M grating.



Echelle Scattered Light Correction

As illustrated in Figure 5, STIS echelle spectra reduced with a standard one-dimensional background subtraction algorithm are subject to zero-point errors, especially in the cores of strong absorption lines. An “algorithm” parameter has been added to the **x1d** spectral extraction task in STSDAS/CALSTIS. Changing this parameter from “unweighted” to **sc2d** enables a new two-dimensional background subtraction algorithm that was designed by Don Lindler (Advanced Computer Concepts, Inc.) and Chuck Bowers (Goddard Space Flight Center). Figure 5 shows the dramatic improvement achieved with the use of this new algorithm. Figure 6 summarizes the fractional error in saturated line cores as a function of wavelength and grating for both algorithms. Errors for the medium resolution gratings are comparable to errors for the high resolution gratings.

Figure 5: Comparison between the standard 1-D and the new 2-D background subtraction.

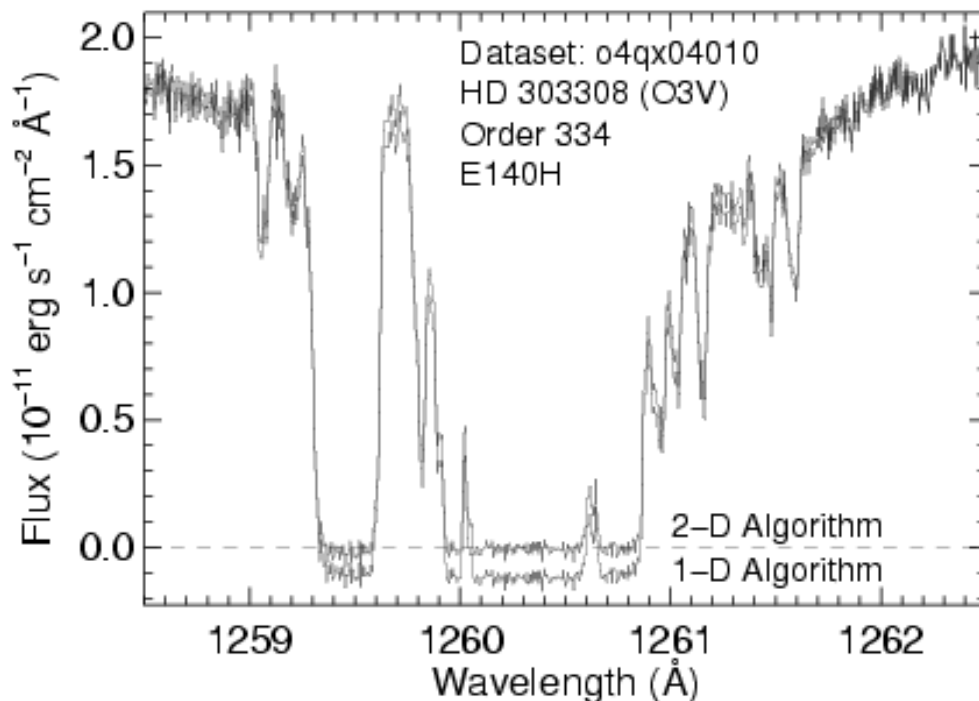


Figure 5: STIS echelle spectrum of a saturated interstellar absorption line. One-dimensional interpolation of the scattered light between orders yields a poor estimate of the background beneath an order. In this case, the standard 1-D background subtraction algorithm yields an error in the line core that is 9% of the continuum flux. The newly implemented 2-D

background subtraction reduces the error in saturated line cores by a factor of ten.

Figure 6: Comparison between the errors of the two methods.

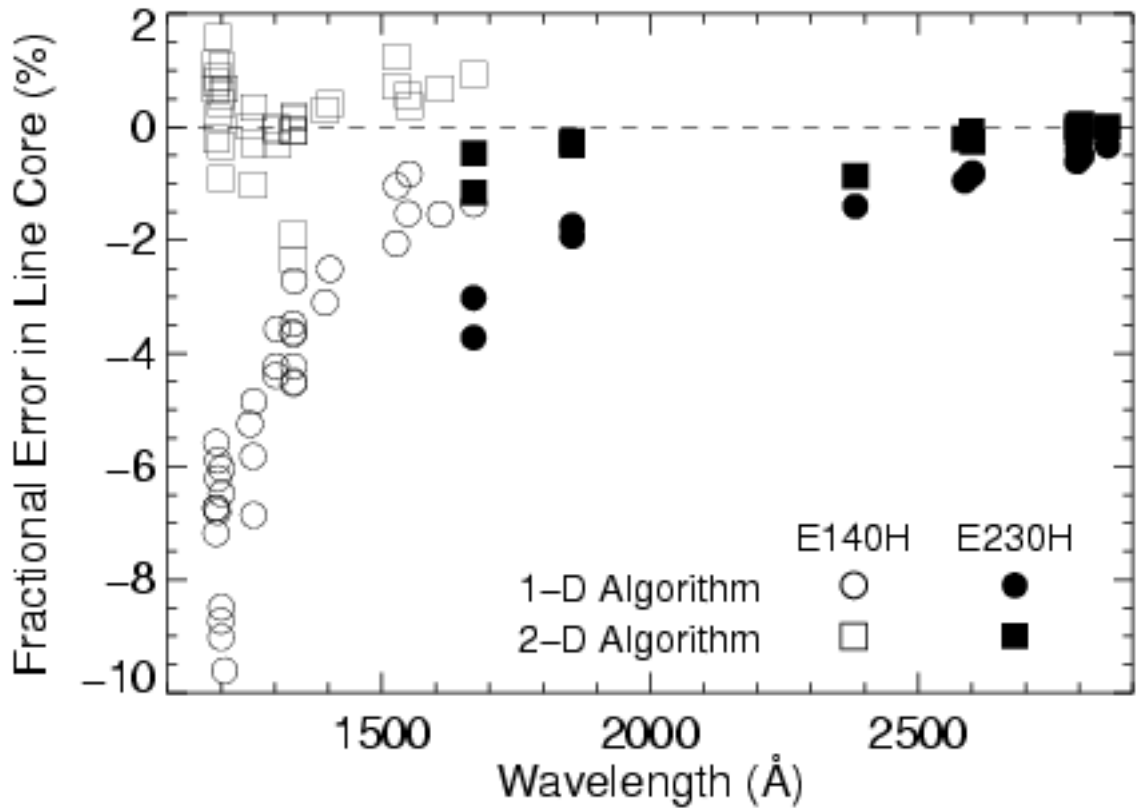


Figure 6: Errors in saturated interstellar line cores, relative to the continuum flux. One-dimensional background subtraction (circles) yields errors that rise to 3.5% at the blue end of E230H spectra and 9% at the blue end of E140H spectra. Two-dimensional background subtraction reduces errors to at most 1% for all wavelengths and gratings. Formal error bars are typically smaller than the plot symbols.

The enhanced **x1d** task is not in the version of STSDAS currently available (as of Dec. 2000), but it will be part of the STSDAS release scheduled for early 2001. In the interim, the new **x1d** task can be run as a user installed package named **sc2d**, which is available for download from:

www.stsci.edu/cgi-bin/stis?stisid=568&cat=calibration&subcat=escat

In early 2001, new requests for STIS echelle data will be reprocessed automatically, using the new two-dimensional background subtraction algorithm. This will be true of all requests for new or archival echelle data.

Briefly, the new algorithm of Lindler and Bowers works as follows: a 2-D raw image is fit with a 2-D model, reconstructed at each iteration from the best current estimate of the extracted spectrum folded through a semi-empirical simulation of STIS optical properties. Self-consistency between the 2-D model and the extracted spectrum is achieved via iteration. An analogous model containing only scattered light is then constructed using only the echelle scatter outside an 11 pixel wide vertical window centered on each order. This 2-D scattered light model is subtracted from the raw data and the final spectrum is obtained using standard 1-D extraction.

Construction of the 2-D model during each iteration involves several steps. Counts in the 1-D extracted spectrum are mapped back to their idealized origin in hypothetical echelle orders that extend beyond the edge of the physical detector. Echelle scatter is modelled by redistributing extracted counts along diagonal lines of constant wavelength, using echelle line spread functions. Post-echelle smearing along columns is modelled by independently convolving each column with a smoothing kernel. Scattering due to the aperture truncated telescope PSF, isotropic detector halo, and pre-echelle scattering by the cross-disperser are treated by 2-D convolution with a kernel constructed from these components.